CAN SEISMIC VELOCITY STACKING ERRORS RESULT IN THE LOW-FREQUENCY SHADOW?

By

Umit Serhan Inan

A THESIS

Submitted in partial fulfillment of the requirements for the degree of

MASTER OF SCIENCE

In Geophysics

MICHIGAN TECHNOLOGICAL UNIVERSITY

2016

This thesis has been approved in partial fulfillment of the requirements for the Degree of MASTER OF SCIENCE in Geophysics.

Department of Geological and Mining Engineering and Sciences

Thesis Advisor:	*Prof. Wayne D. Pennington*
Committee Member:	*Prof. Roger M. Turpening*
Committee Member:	*Assoc. Prof. Gregory P. Waite*
Department Chair:	*Prof. John S. Gierke*

Table of Contents

List of Figures

List of Tables

Acknowledgements

First of all, I would like to express my deepest and most sincere appreciation to my advisor, Professor Wayne D. Pennington, who has always been encouraging, patient and helpful. His guidance and support, both academic and personal, have been inspiring for me.

I also would like to thank my committee members Professor Roger Turpening and Professor Gregory P. Waite.

I want to thank Colorado School of Mines for Seismic Un*x, and CGG for providing Hampson-Russell.

I would like to thank my dear friends Charlie Breithaupt and Karl Campbell, for their friendship and help, which made this experience enjoyable. This past 2 years would not be same without them. I also want to thank Ender Karakus for his support and help during my time here.

I would like to thank Ali Cankurtaranlar for always being helpful and supportive.

I am deeply grateful to my wonderful mother, father and brother. Thanks to their absolute belief in me and infinite love, I was able to accomplish this.

I also would like to express my gratitude to my aunt Gonul Blalock, for being the best aunt there could ever be. I could not even imagine getting through this 2 years without her. I would like to thank my uncle Troy Blalock for always being there for me.

Lastly, my incredible fiancée. All the words in the world could not even begin to describe her support. There is no way, nor there would ever be, that I could express my appreciation for everything she has done, especially despite long distance. It is absolutely thanks to her company, everything is better.

Abstract

The low-frequency shadow is the area on reflection seismic data, underneath gas reservoirs, that exhibits anomalously low frequency. This phenomenon has been related to the highly attenuating nature of the gas reservoir, which could explain the low-frequency shadows observed underneath extremely thick reservoirs, but not the ones underneath thin reservoirs. There are several other mechanisms that could be responsible, however detailed analysis of these possible explanations is yet to be found in the literature.

The main focus of this research is to test the possible contribution of stacking of offset seismic data, namely, their mis-stacking, to the generation of the low-frequency shadow. Due to the fact that thin gas reservoirs, especially reflections from the thin sand layers, are easy to miss during velocity analysis, reflections from the base of the reservoir and from layers immediately below it may not be stacked properly – the lower velocity associated with the reservoir itself may not have been identified in the velocity analysis. In order to understand effects of stacking on the frequency content of a seismic data, and specifically on the reflectors beneath the reservoir, several tests are performed on synthetic seismic data, generated with ray tracing in acoustic models. Spectral analysis methods, such as the Fourier Transform and spectral decomposition are used to better understand the changes in frequency content of the data.

Comparison of properly stacked and mis-stacked horizons showed that the frequency content of a horizon is closely related to the quality of the stacking. This could cause a shift in the peak frequency and a loss of high frequencies, either of which could be identified as a low-frequency shadow.

1. Introduction

The low-frequency shadow is explained by Taner et al. (1976) as a change in frequency content of reflections underneath gas or condensate reservoirs towards lower frequencies. They also noted that even though this phenomenon is observed immediately underneath the reservoir, deeper reflections appear normal. The low-frequency shadow has been in the literature more than 30 years, nevertheless there is little published research about it. Because of this, the low-frequency shadow is still an empirical observation and the mechanism behind it is unknown. Therefore, the conditions under which one should expect to observe a low-frequency shadow are not clear and formulating a quantitative relation to reservoir parameters is currently impossible.

A frequently used explanation of low-frequency shadows is based on attenuation of elastic waves resulting from partial gas saturation. To be able to better understand the effects of attenuation on seismic amplitude with changing thickness, velocity and signal frequency, a simple analytic approach is used in this study.

As seismic waves travel through the earth, they undergo processes that reduce wave amplitudes. Many of these processes, such as geometrical spreading, reflection, transmission, mode conversion and scattering, result in an apparent attenuation; they are elastic processes, in which the energy is conserved. On the other hand there is an

anelastic process of intrinsic attenuation, through which seismic energy is converted to heat.

The physical parameter used to describe intrinsic attenuation is the Quality Factor, or Q. Q, as defined by Knopoff (1964), is a dimensionless physical parameter inversely related to attenuation; a higher Q means lower attenuation and lower Q means higher attenuation. Equation 1 shows the relation between Q and energy loss (Knopoff, 1964). ΔE represents the amount of energy attenuated per cycle in a certain volume and E is the energy of the wave at the start of that cycle.

Eq. 1.

$$\frac{2\pi}{Q} = \frac{\Delta E}{E}$$

Several different approaches can be found in the literature for Q. We used the constant-Q model by Kjartansson (1979), which, as suggested by Yilmaz (1987), is a convenient one to use, especially for the frequencies present in seismic reflection data.

We can re-write the equation for amplitude spectrum of inverse Q filter and get equation 2 to calculate effects of attenuation on amplitude (A), in terms of frequency (f), velocity (V), thickness (z) and Quality Factor (Q) (Yilmaz, 1987).

Eq. 2.

$$A^{-1}(f, v, z, Q) = \exp\left(-\frac{\pi f z}{QV}\right)$$

In order to examine the effects caused by the reservoir, thickness, velocity and Q values are used as parameters to define a reservoir. We analyze these in reference to the amplitude of a wave as it encounters the top of the reservoir.

Figure 1 shows the effects of different Q values on amplitude loss for a range of frequencies, within the usual ranges for seismic surveys. The thickness of the reservoir is 200 m and its velocity is 3000 m/s. We note that the attenuation of a signal can take place in a model such as this, but it is only significant for very low values of Q or for very high frequencies. It can be seen from the figure that even when Q is as low as 20, the amplitude of the signal remains significant at all frequencies. The difference in signal attenuation between high and low frequencies is the basis of the low-frequency shadow; as an example, we see that for a Q of 50, the loss at 60 Hz is 22%, and the loss at 20 Hz is only 8%; analysis methods that compare signal strengths at these frequencies will notice an apparent relative strengthening of the low-frequency component of the signal.

Figure 2 shows solutions to equation 2 in another form, by identifying the necessary thicknesses and Q values to attenuate 90% of the amplitude as a function of frequency. Velocity of the reservoir is again assumed to be 3000 m/s. We observe that extremely thick reservoirs are required to nearly eliminate the signal at most frequencies.

Lastly, a set of reservoir thicknesses, including some unrealistic values, is investigated to identify the values of Q needed to retain 50% of the original amplitude (Figure 3). We note that, even with low Q values, the limited thickness of many

reservoirs is not sufficient to create a strong low frequency shadow. It may be useful to recall that a Q of 6.28 (2π) results in a 100% energy loss of signal in one wavelength and a Q of 12.57 (4π) in a 50% energy loss; the wavelength of a 30 Hz signal in this example is 100 m (from Equation 1). Very low values of Q may account for low-frequency shadows, but these are surprisingly low values indeed.

These observations, and those by Castagna et al. (2003) and by Barnes (2013), lead one to conclude that low-frequency shadows by intrinsic attenuation might be considered logical for extremely thick reservoirs, but do not seem sufficient to explain the observed low-frequency shadows under thin reservoirs. Ebrom (2004) presented a list of ten mechanisms that could explain the low-frequency shadows, especially the ones under thin reservoirs. One of the mechanisms presented in that paper is "mis-stacking due to too coarse velocity picking" (Ebrom, 2004). An examination of this possibility for the case of thin reservoirs forms the main focus of this study.

Preparing stacked sections from a typical seismic survey requires many processing steps, all of which have been greatly improved over time. Nonetheless, velocity analysis still involves a great deal of human judgment, and its results may vary from operator to operator. Because velocity analysis is a highly time-consuming process, it is performed only along a grid of locations, and not each common midpoint gather. This regular grid of locations might be too sparse to detect the reservoir, and the velocity estimates may represent neighboring (water-saturated) formations, rather than the reservoir itself, or the specific reflectors used may not represent the

immediate base of the reservoir rock even if the analysis grid-point is at the reservoir location. As a result, the velocity analyses may misidentify the optimal stacking velocity within the area immediately beneath the reservoir. Because gas reservoirs in low-velocity formations often exhibit lower velocities than the same formations fully saturated with water, the velocities used for stacking may be higher than appropriate in the area immediately beneath the gas reservoir.

In order to illustrate the effects of mis-stacking, we first use a simple approach: the summing of two wavelets with varying time differences. A band-pass zero-phase wavelet is defined with the corner frequencies of 5, 10, 40 and 45 Hz. To perfectly stack two identical wavelets, the time shift between the two wavelets should be zero, and mis-stacking will occur if there is a non-zero time shift. In Figure 4 we see the results of two identical wavelets are being stacked with time shifts from 0 ms to 12 ms. With a time shift of 12 ms, the amplitude at 40 Hz is reduced to zero (a half-period shift), and at all lower frequencies and/or smaller time signals, the various frequency components lose some fraction of their amplitude. The effect is greater at higher frequencies up to the half-period time shift.

This study then assumes a stronger modeling approach to investigate the creation of a low frequency shadow due to the effects of mis-stacking using more-realistic models with greater fold. Several different models are generated using ray-tracing, based on seismic ray theory (Cerveny, 2001). We start with simple models and add increasing complexity. As a starting point, a simple flat-layer model is generated with

a finite gas reservoir in the middle of the model. Next, a more complex anticline model is generated with a gas reservoir at the peak of the anticline. At first, we assume no intrinsic attenuation occurs ($1/Q = 0$), but then several different versions of the anticline model are created using finite values of Q. We note that we ignore some physical aspects of true seismic reflection surveys, including multiple reflections, converted waves and scattering effects. This approach allows the effects of stacking to be seen in isolation from any other contributing cause.

2. Methods

We employ several different modeling methods with the intention of investigation of the effects of stacking on the low-frequency shadow in this study. Several different subsurface models are created, based on environments from which low-frequency shadows have been reported. Forward modeling using ray tracing techniques in Seismic Un*x creates synthetic data in the form of shot gathers. To be able to investigate the effects of stacking, synthetic models are stacked both using "correct" (including the low-velocity gas layer) and "incorrect" velocity profiles, which are generated using V_{RMS} velocities based on the input model. Flat-layer models are used for many of the examples, but an anticlinal model, sometimes incorporating finite values of Q, is also studied. The analysis method includes examination of amplitude

spectra of isolated horizons as well as common-frequency gathers (from spectral decomposition).

In this section, we present the varying models and analysis methods, but do not yet present the results of those models or analyses; that will come in a later section.

2.1. Forward Modeling

Parameters in the numerical model are selected that are similar to a typical seismic survey. A Ricker wavelet with 40 Hz peak frequency is used (Figure 5), providing sufficient vertical resolution to display thin (~100 m thick) sand layers. Sample rate 1 ms and number of samples varies depending on the model. To increase the fold number, split spread shot geometry is used with 60 receivers for each shot at 25 m spacing with initial offset of 25 m. The number of shots varied depending on the model. More detailed survey parameters are given for each survey in Appendix A.

After generating the synthetic shot gathers, random noise (signal-to-noise ratio of 20:1) was added to the data and filtered with corner frequencies of 0 Hz, 10 Hz, 75 Hz and 90 Hz to be similar to the spectral content of the wavelet. CDP (common depth point) sorting was done prior to NMO (normal move out) correction and stacking. A mute was applied to the traces that were stretched by more than 50 %.

Reservoir and formation parameters were selected to resemble the areas where low frequency shadows are observed. The general parameters used in most models are

explained below, and the details of specific structures and layer parameters will be provided with the presentation of each model.

The reservoir parameters represent a sandstone with 30% porosity with 70% gas and 30% water saturation. The density and modulus of the pore fluid was calculated using Batzle and Wang (1992). The velocity of the sandstone matrix was selected from the range given in Mavko et al. (2009) and density of quartz was used for the matrix (grain) property. The Raymer-Hunt-Gardner relation was used to calculate the velocity of the water saturated gas sand from matrix velocity and fluid velocity (Raymer et al., 1980). Then, velocity and density of the reservoir were calculated using fluid substation with P wave modulus approach (Gassmann, 1951). Since most of the gas reservoirs involved in low-frequency shadows are also identified by their "bright spot" reflection, we assumed higher-impedance overlying layer properties. Underlying layers were designed to generate small positive reflections. Density and velocity of the non-reservoir layers were calculated using Gardner's relation (Gardner et al., 1974). A bottom layer (basement) is always modeled in order to generate a strong positive reflection. Detailed parameters for subsurface models for each model are given in the Appendix B.

Flat Reservoir Model

As a simple approach, a flat-layered model with a gas reservoir in the center is generated (Figure 6). The first layer is intended to represent a shale of higher

impedance (both velocity and density) than the underlying sand layers. The second layer is a sand with different fluids in pores, representing the potential reservoir. In the central 2 km (of the 8 km wide model) the sand is 70% gas 30% water saturated, creating the gas reservoir, and sands to its two sides are 100% water saturated. Underneath there are 10 water-saturated sand layers, with increasing velocities and densities and changing thicknesses, followed by a faster and denser layer with parameters similar to first layer, and finally a basement layer.

Varying Depth Model

In order to understand the effects of incorrect stacking velocities on the amplitude spectrum of the reflected signal, a varying-depth model (for V_{RMS}) is created (Figure 7). This is similar to the flat reservoir model, but instead of using a finite width reservoir, the second layer consists of gas sand for the entire width of the model. Underneath the second layer, there are two water-saturated sand layers; the first one is 100 m thick and second one 2500 m thick. Deeper still is the basement.

The point (two-way travel time, or depth) at which the velocity analysis is made is changed in repeated cases -- it moves deeper in 0.2 sec (326.5 m) increments (Figure 8). Thus, the shallowest measure is made immediately beneath the gas reservoir. But with increasing depth in each model, the V_{RMS} is calculated at greater distances (depths or two-way times) from the base of the gas reservoir, and incorporates increasing thicknesses of water sand in its calculation. In addition to changing the

velocity value, also the velocity-analysis depth moves down, which increases the error in NMO correction of the reflector, which is always the same. Therefore, the error between “correct” and “incorrect” gets larger.

Anticline Model

The most realistic model created is the anticline model (Figure 9). The peak of the anticline is a gas reservoir, with 150 m thickness and 1400 m width. There is an overlying layer representing the overlying shale. Similar to the first flat-layered models, there are 10 water saturated sand layers (conformable to the anticline) under the reservoir and a basement layer.

Furthermore, because attenuation is ignored for all these models (in addition to the original anticline model) 4 different models are created with changing Q values in the reservoir zone. This way, the effects of attenuation on a seismic section can be observed and results of different Q values can be compared. Q values used for the reservoir are, 100, 50, 25 and 10.

2.2. V_{RMS} Velocities and Stacking

In real field data, one needs to perform a velocity analysis in order to obtain moveout parameters. Rather than yield this study to subjective, interpreter-dependent judgments, we use root-mean-square velocities (V_{RMS}, Equation 3) to provide the

velocities needed for NMO correction (Yilmaz, 1987) and stacking. In order to study the effects of stacking on the generation of low-frequency shadows, we used both correct (incorporating the reservoir layer) and incorrect V_{RMS} values.

Eq. 3.

$$V_{RMS} = \sqrt{\frac{\sum_i V_i^2 t_i}{\sum_i t_i}}$$

For the flat reservoir model, two different velocity profiles were needed to create a correct stacked section because there are vertical sections that contain only water sands, and vertical sections that contain the gas reservoir. The only difference in those profiles is in the second layer, which contains the reservoir zone in the central portion of the model. For the "correct" analysis, the velocities appropriate at all depths were used everywhere; for the "incorrect" analysis, the velocities appropriate for the sides of the model, without the gas zone, were used everywhere, (this, also is an incorrect velocity model beneath the gas reservoir).

Similarly, V_{RMS} velocities are used for correct and incorrect stacking for the varying-depth model. Recall that the velocity analyses are performed at greater times (depths) while correct V_{RMS} velocities are used for each such point; this implies that the layer(s) immediately beneath the reservoir are stacked with slightly incorrect velocities, down to the point where the next analysis was performed. With increasing time (depth) between the top of the reservoir and the analysis point, a greater number of reflectors will be affected, but the error in the velocity will decrease. Figure 10A

presents the V_{RMS} velocities beneath the water-sand case and the gas-sand case with larger intervals between the reservoir and analysis point; Figure 10B shows the difference between those velocities. As can be seen in the figure, the two V_{RMS} velocities get closer as the thickness of the layer increases.

On the other hand, computed V_{RMS} velocities are not used for stacking for the anticline model; instead, traditional velocity analysis is performed, providing the "correct" velocities. However, to be able to observe the effects of stacking, a model identical to the gas-reservoir anticline model is created without the gas reservoir, and a second velocity analysis is performed on that model, providing the "incorrect" velocities to be applied to the original anticlinal model. That is, similar to our processing of the flat reservoir model, two stacked sections are created here, one with "correct" velocities from the model with the gas zone, and another with "incorrect" velocities.

2.3. Spectral Analysis

Spectral analysis is often used to demonstrate the low-frequency shadow, and many techniques have been shown to be useful (Castagna et al, 2003). Two different spectral analysis techniques are used in this study: conventional amplitude spectrum from a Fast-Fourier Transform (FFT) over short time windows; and spectral decomposition applied to the seismic section.

Amplitude Spectrum

Amplitude spectra of seismic data can provide valuable information about the frequency content of the data. The usual FFT, however, makes some assumptions to overcome the analytical requirement of an infinite time series. In practice, this results in a limit to the density of frequencies analyzed – shorter time series can have fewer analysis points in the frequency band of interest. In order to assess the frequency content of the reflected arrivals in our varying-depth model, we selected a one-second time window and used FFT calculation to obtain the amplitude spectrum. This time window includes a single reflector, while being of sufficient length to provide adequate sampling of frequencies. The change in the frequency content of the reflector varies depending on the depth at which velocity analysis is done; note that the depth (time) of the reflector itself does not change, while the depth (time) of the velocity analysis does.

Spectral Decomposition

A typical seismic section will have a bandwidth of a few Hz to ~100 Hz, which is a significant bandwidth to capture in simple displays of seismic sections. Spectral decomposition is a strong tool allowing interpreters to view the seismic section from another point of view, providing considerable frequency information (Partyka et al., 1999). There are many different spectral decomposition methods described in the literature with different advantages and short comings (Castagna et al., 2003).

The method used in this study is the Complete Ensemble Empirical Mode Decomposition (CEEMD); this decomposes wavelet into a set of components called Intrinsic Mode Functions, based on a similar method, the Empirical Mode Decomposition (EMD) (Torres et al., 2011; Han and van der Baan, 2013). CEEMD is reported to offer a higher time-frequency resolution than other spectral decomposition techniques, which emphasizes geologic features more distinctly (Han and van der Baan, 2013).

CEEMD was applied to stacked sections of all the models presented in this study, and constant-frequency sections were generated for 10, 20 and 30 Hz. Constant frequency sections provide a view of the data in the form of (spectral) amplitude for that specific decomposed frequency (10, 20, and 30 Hz in our case) as a function of two-way travel time.

3. Results

Flat Reservoir Model

Synthetic seismic data were created using the flat reservoir model and stacked using two different velocity profiles are shown in Figure 11. Figure 11A is the correctly stacked section, stacked using correct V_{RMS} velocities for both the gas and water zones. Figure 11B is the incorrectly stacked section, stacked using just the water zone V_{RMS} values for both the gas zone and water zone. Figure 11C shows both correct and

in correct stacked sections in a split image, zoomed in to the reservoir zone. The effect of mis-stacking in this display is subtle: the reflections are slightly wider in the incorrect stack. The effects of mis-stacking disappear as reflectors get deeper, because the V_{RMS} velocities are closer (Figure 10).

A closer look at the reflections from the base of the first sand layer beneath the gas reservoir can provide some additional insight. Because incorrect V_{RMS} velocities for the water zone are used in the gas zone, the reflections are not precisely aligned after applying moveout for the (incorrect) velocities, as shown in Figure 12A. The stacked traces from those NMO-corrected CDP gathers are also shown (Figure 12B), and their amplitude spectra compared (Figure 12C). While the total amplitude loss can be seen as a result of mis-stacking, a more significant distinction is the difference observed in the high frequencies, relative to the low frequencies. The major part of the loss in amplitude comes from the high frequencies.

Common-frequency sections are created using spectral decomposition. First, we look at correctly stacked section, and then incorrectly stacked sections. The 10 Hz and 30 Hz common frequency sections for correctly stacked section are displayed in Figure 13 (together with the stacked section for reference). Figure 14 shows the stacked section, the 10 Hz common-frequency section and the 30 Hz common-frequency sections for the incorrectly stacked sections. In this case, we observe high amplitude values (at 10 Hz) surrounding the reservoir area and note that these amplitudes are larger in the incorrectly stacked section. The important comparison to be made is

between the amplitudes at 10Hz and at 30Hz for each section, where it becomes apparent that the incorrectly stacked section is much richer in lower frequencies (relative to the higher frequencies). (We notice that a 50 ms upward time shift is observed in the 10 Hz sections, apparently an artifact of the CEEMD processing, but this is not apparent in the 30 Hz sections.)

Varying Depth Model

The varying-depth model is designed to show the effects of mis-stacking by shifting the point at which the velocity analysis is done; recall that in this case, the velocity analysis always includes the gas zone. Figure 15 shows the amplitude spectrum of the bottom of the gas reservoir for each of several (deeper) velocity-analysis points. As the time delay between the reflector and the point of stacking gets larger, the (stacked) peak (spectral) amplitude gets smaller and the peak frequency shifts towards lower frequencies. More significantly, however, it should be noted that the decrease in amplitude is much greater at higher frequencies (such as 60 Hz as shown by the red arrow), than at lower frequencies (for example, the decrease is negligible at 20 Hz).

Anticline Model

The anticline model is the most geologically realistic model used in this study. Figure 16 presents the correct and incorrect stacked sections in a split display, side by side.

Again, the difference is very subtle, and mostly apparent in a slight broadening of the reflection at the base of the reservoir.

In addition to this stacking comparison, the anticline model is also used to compare the differences created by varying Q values within the reservoir. Figure 17 shows the central portions of the stacked seismic sections created from models using different Q values (100, 50, 25, and 10). It can be seen that as the Q value decreases, reflections underneath the reservoir lose amplitude and most importantly, despite the high Q values of underlying sand layers, the amplitudes do not recover with greater depth.

Finally, spectral decomposition is employed once more to see the effects of Q on a certain frequency. Figure 18 shows the 10 Hz common-frequency sections and Figure 19 shows the 30 Hz common-frequency sections for models which have Q values 100, 50, 25, of 10 for the reservoir. Similar to the stacked sections, common frequency sections show higher loss of amplitudes for lower Q values. Furthermore, the effect of a low Q zone can even be seen extending all the way down to the reflection from the basement reflector, particularly on the lowest-Q section (Figure 18D and Figure 19D).

4. Discussion

The current popular explanation of the mechanism that creates the low-frequency shadow is attenuation caused by gas. However, a simple analytical approach demonstrated that a typical thin gas reservoir cannot attenuate that much amplitude from the signal, regardless of the frequency. Yet, this does not mean that attenuation does not contribute to generation of low frequency shadows, but it shows the limited role that attenuation may play. Other mechanisms may be important, such as stacking errors as investigated in this study.

Velocity analysis is a process that yields varying results depending on the knowledge and experience of the data processor; it is easy to skip a weak horizon, such as that between the gas sand and an underlying water sand, and performing the analysis on the next (deeper or later) strong-reflecting horizon. We used the V_{RMS} velocity calculation for a varying-depth model and showed that the frequency content of the data may change appreciably. The peak frequency of the data was shifted slightly towards lower frequencies, and we showed that mis-stacking would result in greater loss of high frequencies, one of the characteristics of low-frequency shadows. This becomes particularly apparent in displays of common-frequency sections.

Our models of changing Q values in the reservoir and not the surrounding layers showed that once the signal is attenuated, it does not recover with greater time/depth. By itself this suggests that attenuation alone is unlikely to be the source of a low-frequency shadow.

5. Conclusion

The low-frequency shadow has often been considered to be a hydrocarbon indicator, yet the mechanism behind it has not been understood. General assumptions, such as attenuation from gas zones as a cause, are far from satisfactory, and there may be complex mechanisms behind this phenomenon.

We tested the effects due to stacking errors, and showed that stacking can be an important factor for the frequency content of the resulting seismic section. Picking correct velocities at necessary depths immediately beneath a reservoir would reduce the appearance of the low-frequency shadow, suggesting that not picking such velocities accurately is at least one source.

Overall, attenuation of high frequencies by low Q values in the reservoir is one of the reasons for the low-frequency shadow, however, it is certain that its role is smaller than estimated, and, its effect is very small for thin reservoirs. Also it could be said that, mis-stacking of the reflectors immediately underneath the thin gas reservoirs, plays a role in generation of the low frequency shadow, still, further investigation is needed to estimate its true contribution to this problem.

6. References

Barnes, A. (2013). The Myth of Low Frequency Shadows. (pp. 1-5). Singapore: EAGE.

Batzle, M., & Wang, Z. (1992). Seismic properties of pore fluids. *GEOPHYSICS, 57*(11), 1396-1408.

Castagna, J., Sun, S., & Siegfried, R. (2003). Instantaneous spectral analysis: Detection of low-frequency shadows associated with hydrocarbons. *The Leading Edge, 22*(2), 120-127.

Cerveny, V. (2001). *Seismic Ray Tracing.* Cambridge: Cambridge University Press.

D., E. (2004). The low-frequency gas shadow on seismic sections. *The Leading Edge, 23*(8), 772-772.

E., K. (1979). Constant Q - wave propagation and attenuation. *Journal of Geophysical Research, 84*(89), 4737-4748.

Gardner, G., Gardner, L., & Gregory, A. (1974). Formation velocity and density - the diognastic basics for statigraphic traps. *GEOPHYSICS, 39*(6), 770-780.

Gassmann, F. (1981). Über die elastizität poröser medien. *Vierteljahrsschrift der Naturforschenden Gesellschaft in Zürich*, 1-23.

Han, J., & van der Baan, M. (2013). Emprical mode decomposition for seismic time-frequency analysis. *78*(2), O9-O19.

Knopoff, L. (1964). Q. *Reviews of Geophysics, 2*(4), 625-660.

Mavko, G., Mukerji, T., & Dvorkin, J. (2009). *The Rock Physics Handbook.* New York: Cambridge University Press.

Partyka, G., Gridley, J., & Lopez, J. (1999). Interpretation applications of sprectral decomposition in reservoir characterization. *The Leading Edge*, 353-360.

Raymer, L., Hunt, E., & Gardner, J. (1980). An Improved Sonic Transit Time-to-Porosity Transform, paper P. Trans. (pp. 1-12). SPWLA: Annual Loogging Symposium.

Taner, M., Koehler, F., & Sheriff, R. (1979). Complex seismic trace analysis. *GEOPHYSICS, 44*(6), 1041-1063.

Torres, M., Colominas, M., Schlotthauer, G., & Flandrin, P. (2011). A COMPLETE ENSEMBLE EMPIRICAL MODE DECOMPOSITION WITH ADAPTIVE NOISE. (pp. 4144-4147). ICASSP: IEEE.

Yılmaz, Ö. (1987). *Seismic Data Analysis (Investigations in Geophysics, Vol. 1)*. Tulsa: Society of Exploration Geophysicists.

7. Figures

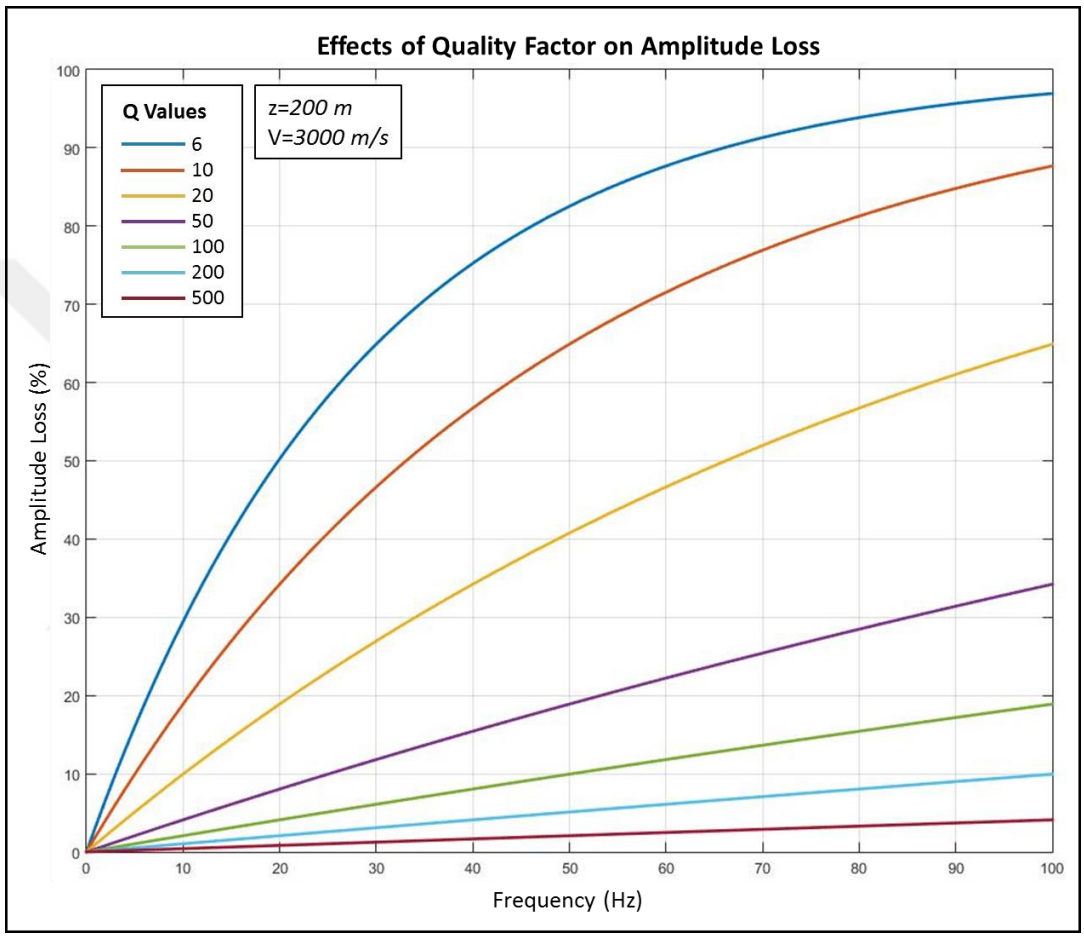

Figure 1: Effects of Quality Factor on Amplitude loss is shown in this figure. Thickness (z) of reservoir is 200 m and Velocity is 3000 m/s. Different Q values are shown with different colored lines. Figure shows that even for low Q values, most of the amplitude of the signal is conserved.

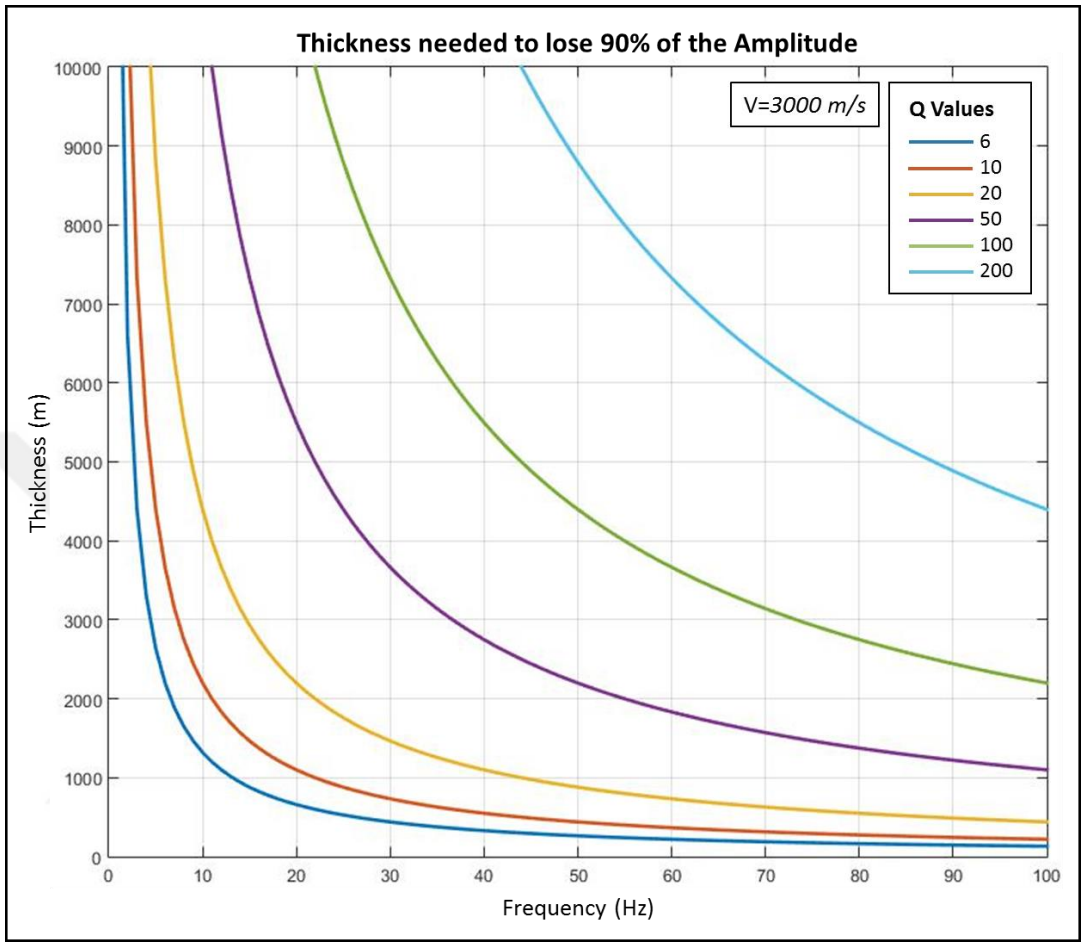

Figure 2: Figure shows the thickness needed to lose 90% of the amplitude. The velocity of the reservoir is 3000 m/s. The legend shows the Q values for different lines. This graph shows how thick of a reservoir is needed to lose 90% of the original amplitude of the wave that enters the reservoir. Notice that, for Q values , which are considered normal for a gas reservoir, reservoir should be thicker than 1 km to filter out the high frequencies from the signal.

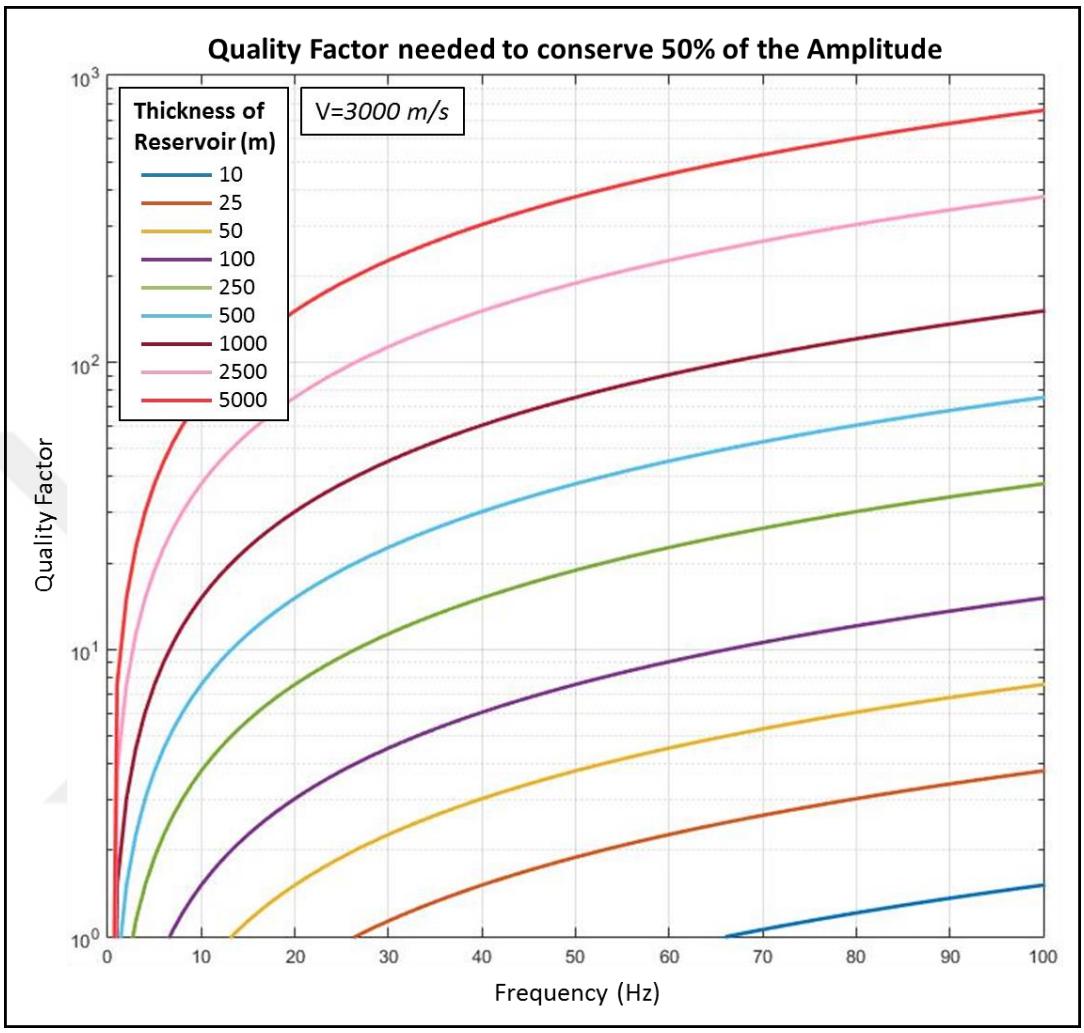

Figure 3: The quality factor values needed to conserve 50% of the amplitude are plotted for different thicknesses. The velocity of the reservoir is 3000 m/s. The legend shows different thicknesses for the reservoir. Y axis shows the Q values in logarithmic scale. For a common thin gas reservoir, that is 100 m thick, even Q values lower than 10, which would be unrealistically low, is enough to conserve half of the amplitude.

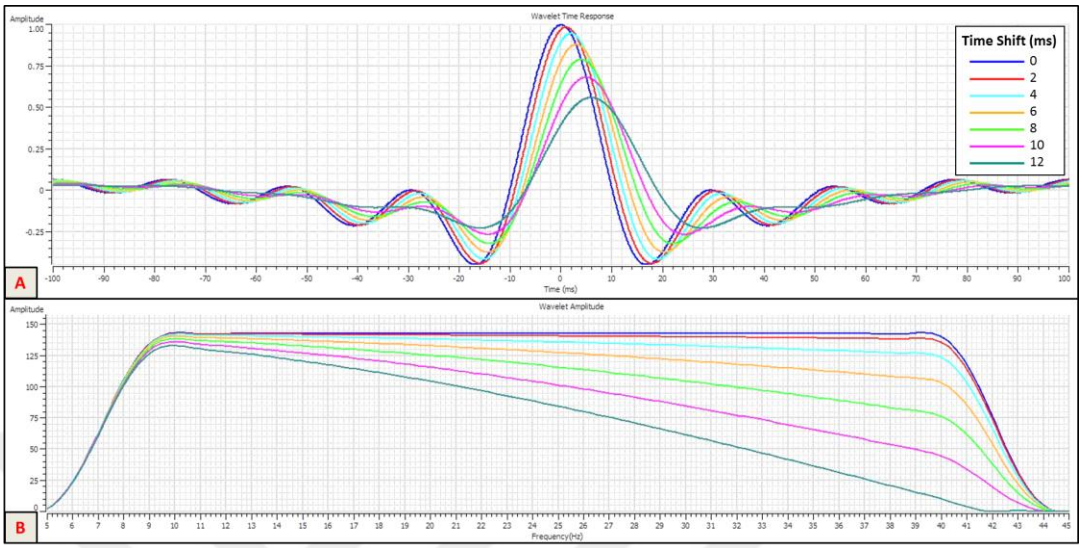

Figure 4: Showing the results for stacking two wavelets with a time shift. The legend shows the different colors representing the stacking results with different time shifts. (A) shows the stacking results in time domain. The amplitude of the wavelet gets smaller as the time shift gets larger. Also wavelets resulting from larger time shifts lost high frequency oscillations. (B) shows the amplitude spectrums of resulting wavelets. Notice that the amplitude loss happens with loss of higher frequencies in the wavelet. Resulting wavelet of stacking with 12 ms time shift has almost zero amplitude for the 40 Hz, which is the highest frequency for the original wavelet.

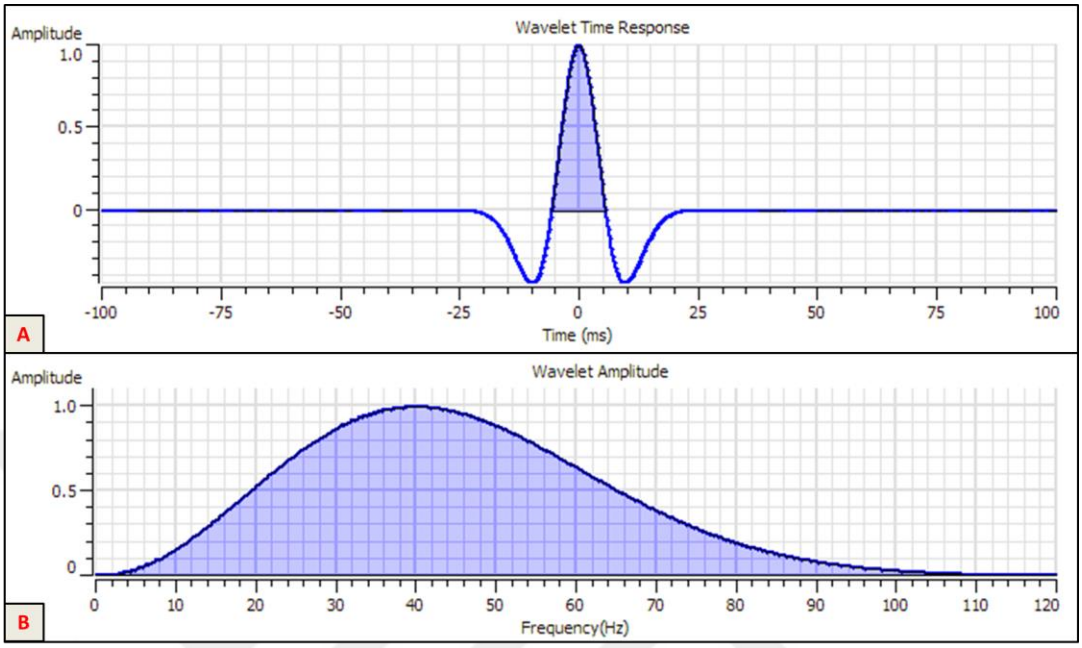

Figure 5: 40 Hz Ricker wavelet used for seismic modeling. (A) shows the wavelet in time domain and (B) shows the amplitude spectrum of the wavelet. As can be seen in the amplitude spectrum, the wavelet has a smooth distribution of amplitude from 0 Hz to approximately 110 Hz , which resembles a seismic amplitude spectrum.

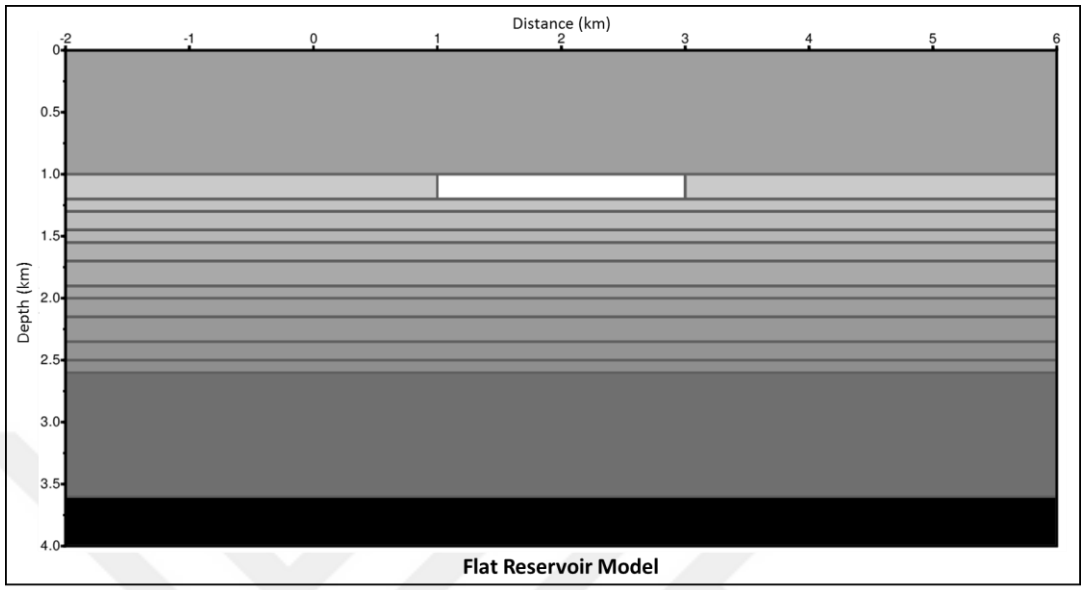

Figure 6: Flat reservoir model. Black color means larger acoustic impedance values, basement layer has the highest velocity and density value, and white is the smallest acoustic impedance value, which in this case is the gas reservoir. Acoustic impedance values in between represented by ranges of gray colors. There is an overlaying faster and denser layer, which can be considered as shale. Underneath the first layer, there are 10 sand layers and underneath those there is another layer which is faster and denser than the last sand layer. Last layer is the basement layer. Sand layers are all saturated with water except the reservoir, which is 70% gas 30% water saturated. With model edges going to -2 km and 6 km. The seismic survey has the ability to reach the full fold of 30, before and after the reservoir.

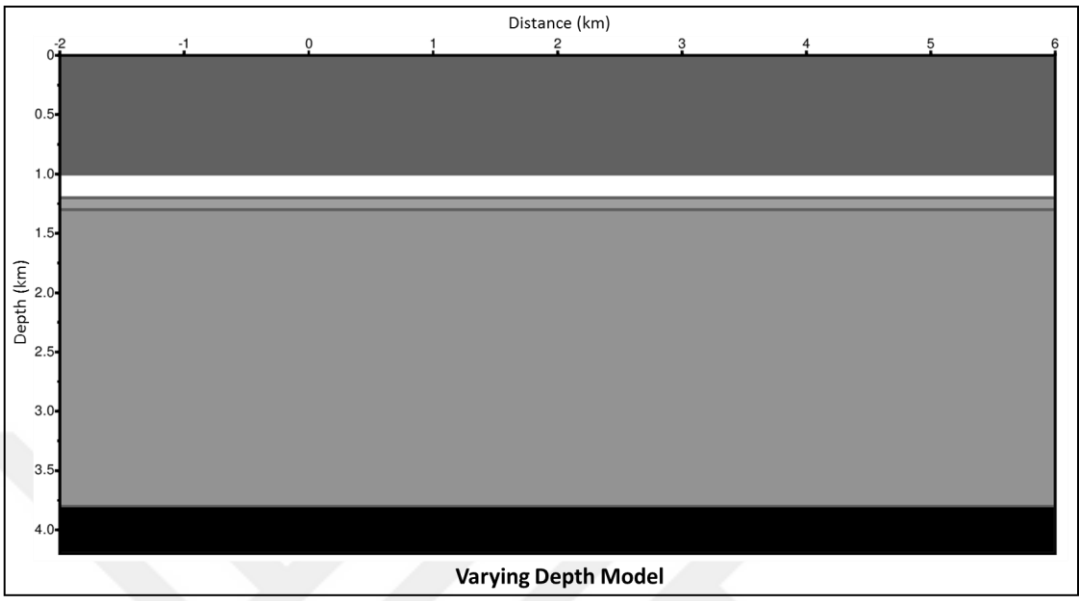

Figure 7: Varying depth model. This model has the overlaying faster and denser layer and a very similar layer as basement. Second layer is the reservoir, gas sand, underneath that there two water sand layers. First one is a thin sand layer with 100 m thickness and second one is a 1500 m thick layer that allows us to vary the depth at which the velocity analysis is done. With one thick continuous layer the window length, which is used for Fourier analysis of the bottom horizon of first sand layer, is chosen to be one second in width, starting before the bottom of the sand layer.

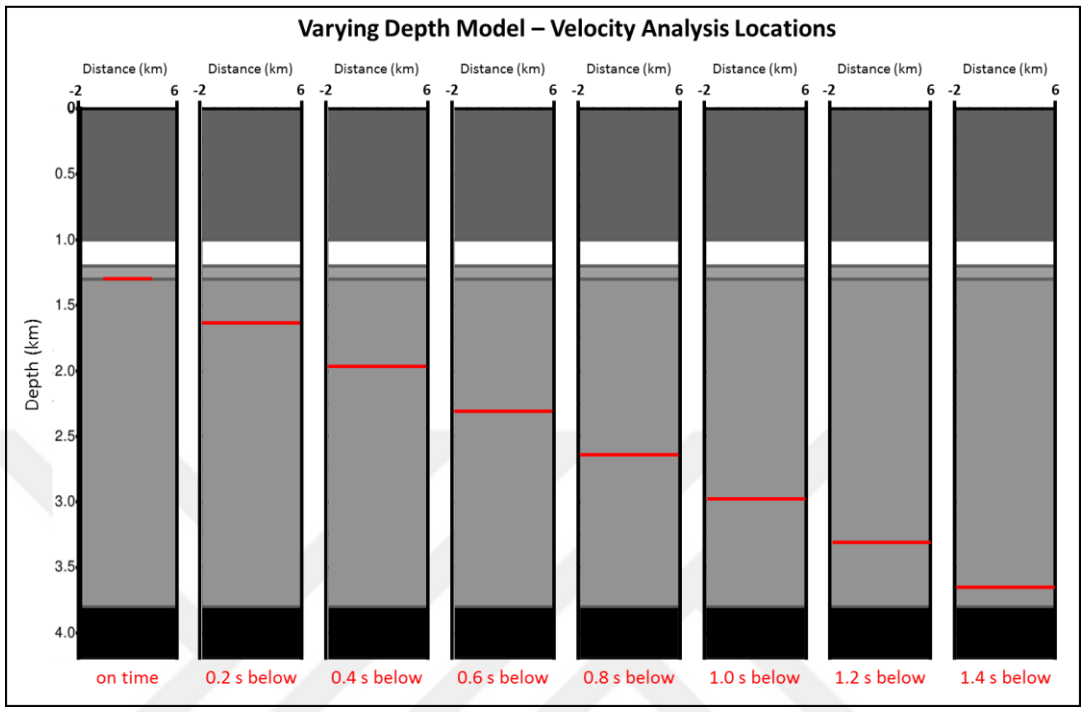

Figure 8: Varying depth model showing the method used for velocity analysis. Red lines show the depths at which the V_{RMS} calculation is done and velocity analysis is applied. First analysis is done at the bottom of the first sand layer underneath the reservoir, after that each analysis is done with 0.2 delay from the one before. Last V_{RMS} calculation is done at a point that is 1.4 seconds below the horizon.

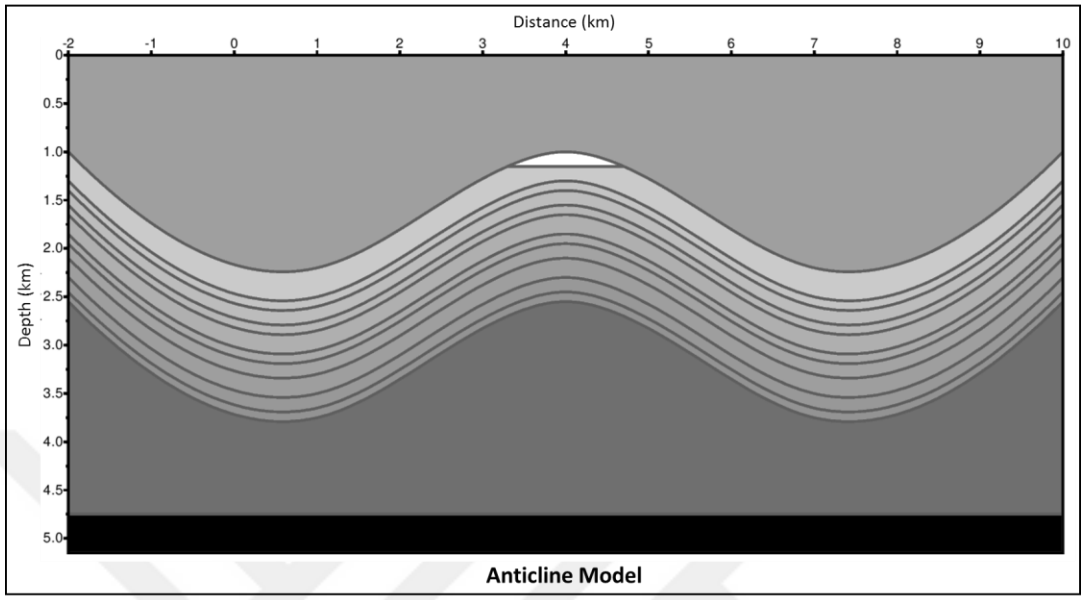

Figure 9: Anticline model. There is a gas reservoir at the peak of the anticline and 10 water sand layers underneath the reservoir. Black represents the highest acoustic impedance and white is the lowest acoustic impedance. First layer is a layer that is faster and denser than the sand layer, which has very similar parameter to the layer underneath the last sand. The black layer is the basement layer. This model is 12 km long, which ensures that CDP gathers reach full fold just after the anticline's limbs start, while keeping a smooth dip for the anticline structure.

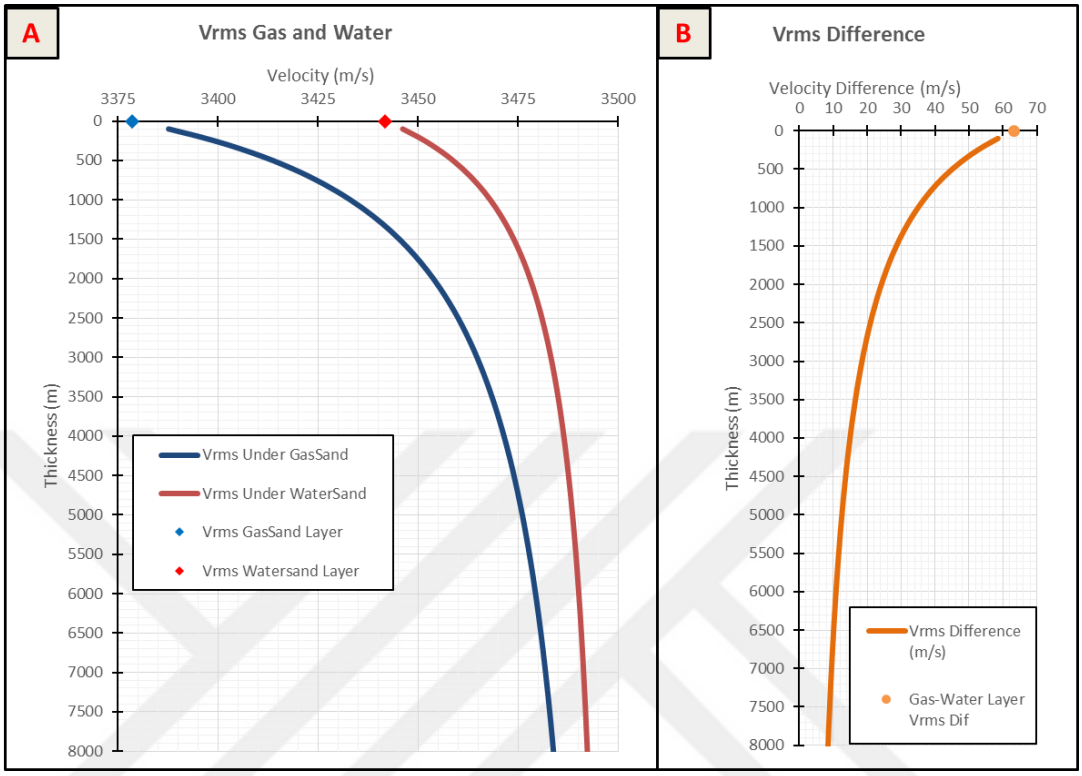

Figure 10: Figure shows the result of V_{RMS} calculations for gas sand and layers underneath and water sand and layers underneath. (A) blue line is the V_{RMS} velocities underneath a gas sand layer and red line V_{RMS} velocities underneath a water sand. Blue dot is the V_{RMS} velocity of the gas sand and red dot is water sand. (B) shows the difference between those velocities. As can be seen in the figures, initially the velocity difference is grater, but as the depth increases, the difference becomes less than significant.

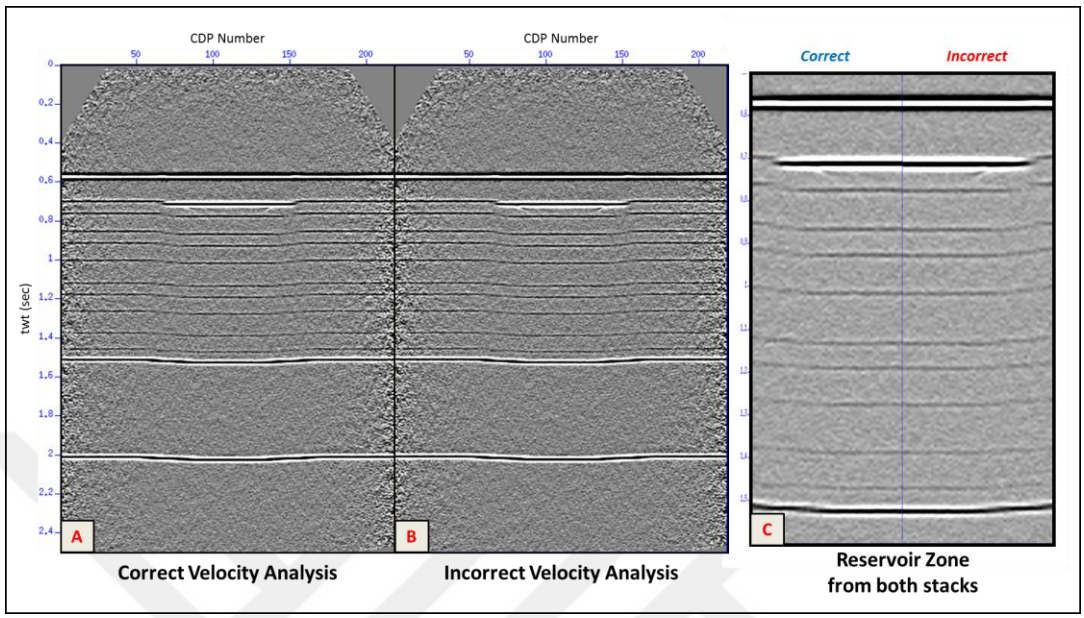

Figure 11: Figure shows the stacked seismic sections generated using the flat reservoir model. (A) is the section stacked using correct V_{RMS} values. V_{RMS} velocity profile is calculated for water sand and layers underneath and V_{RMS} the velocity profile for gas sand and layers underneath are both used for appropriate CDP gather. (B) is the stacked section stacked using only water sand V_{RMS} profile for all CDP gathers. Thus it has been stacked with the wrong values. (C) is created using both stacked sections. Left side is the zoomed area of the reservoir zone's and following horizons' left side from the correct stacked section and right side is the right side of the same area of incorrect stacked section. Namely, it is the reservoir zone, left half stacked correctly and right half stacked incorrectly. Even though it is not obvious, there is a small difference in horizons. Horizons from incorrect side are a little wider, because they are not aligned correctly after NMO correction. Difference of two stacks disappears on deeper horizons, because V_{RMS} velocity difference gets insignificant.

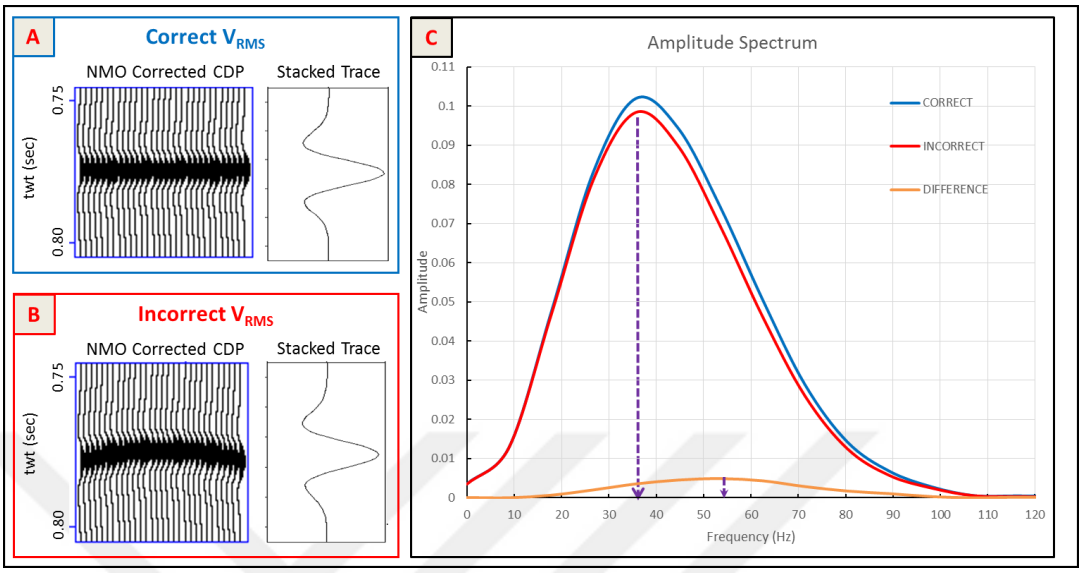

Figure 12: This image shows the comparison of using correct VRMS velocities, calculated for gas sand, on a CMP that is located at reservoir zone and using wrong VRMS velocities, calculated for water sand, on the same location. (A) is the NMO corrected CDP gather using correct VRMS velocity and stack result of that CDP gather. VRMS velocities for gas sand corrected the NMO as it should be and wavelets are aligned properly. (B) is the NMO corrected CDP using incorrect VRMS velocity and stack result of that CDP gather. VRMS velocities for water sand did not correct the NMO and wavelets are not aligned as they should. (C) is the amplitude spectrums of the stacked CDP gathers from both correct (blue line) and incorrect (red line) NMO corrections. Also, the difference between amplitude spectra of correct stacked trace and incorrectly stacked trace is calculated and displayed (orange line). It can be seen that incorrect stacking caused amplitude loss, especially the high frequency part of the signal. Purple dotted lines show the peak frequencies of the amplitude spectrum of the stacked traces and their difference. The difference in the peak amplitude's frequency shows that the loss of amplitude mostly happened in the high frequencies, hence the higher peak frequency of the orange line.

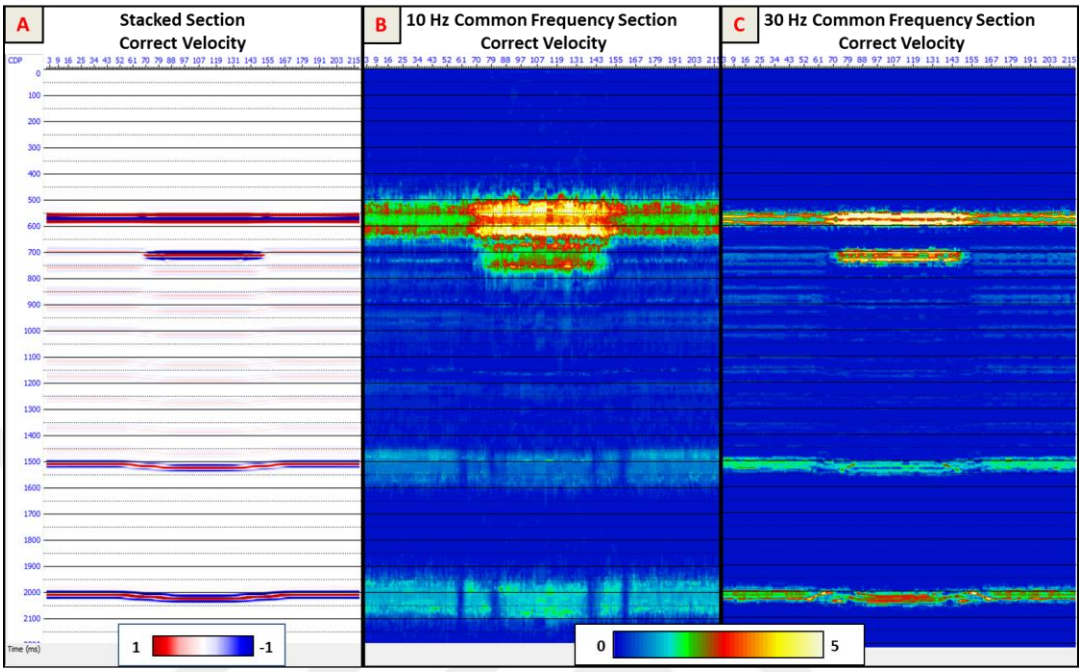

Figure 13: Figure shows the 10 Hz common frequency sections of the stacked sections from flat reservoir model. (A) is the correctly stacked seismic section, mainly as a reference point. (B) is the 10 Hz common frequency section of the correct stacked section. Yellow and red colors are high spectral amplitude and blue is low spectral amplitude. (C) is the 30 Hz common frequency section of the correct stacked section. Same colors are used. Notice that there is a time shift in the amplitude anomalies in the common frequency sections.

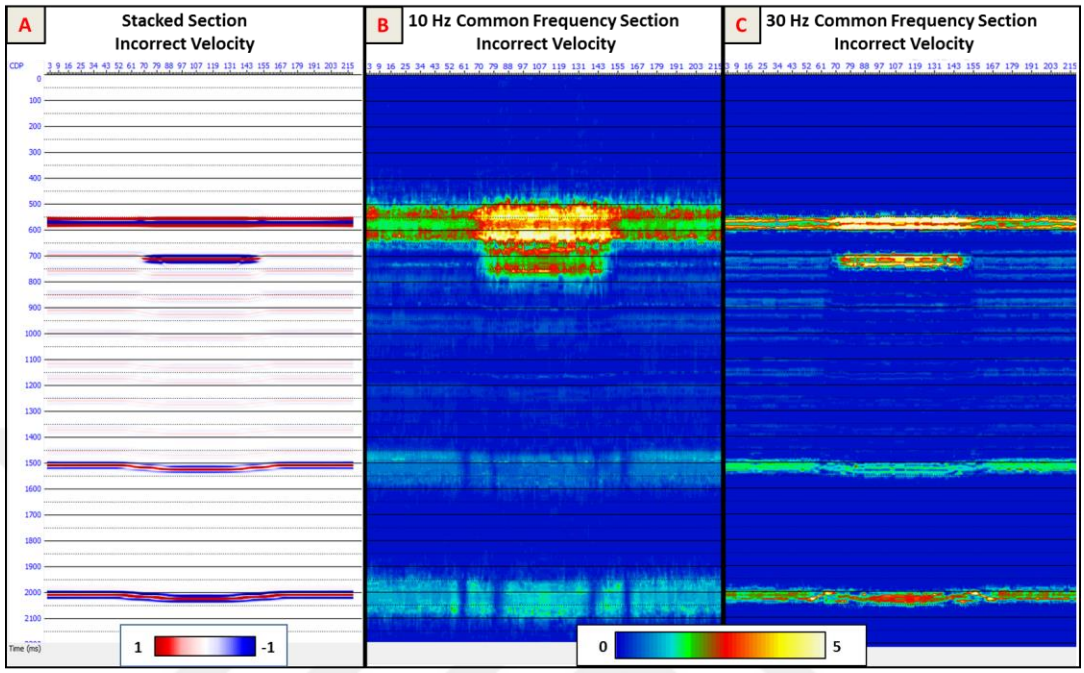

Figure 14: Figure shows the 30 Hz common frequency sections of the stacked sections from flat reservoir model. (A) is the incorrectly stacked seismic section, mainly as a reference point. (B) is the 10 Hz common frequency section of the incorrect stacked section. Yellow and red colors are high spectral amplitude and blue is low spectral amplitude. (C) is the 30 Hz common frequency section of the incorrect stacked section. Same colors are used.

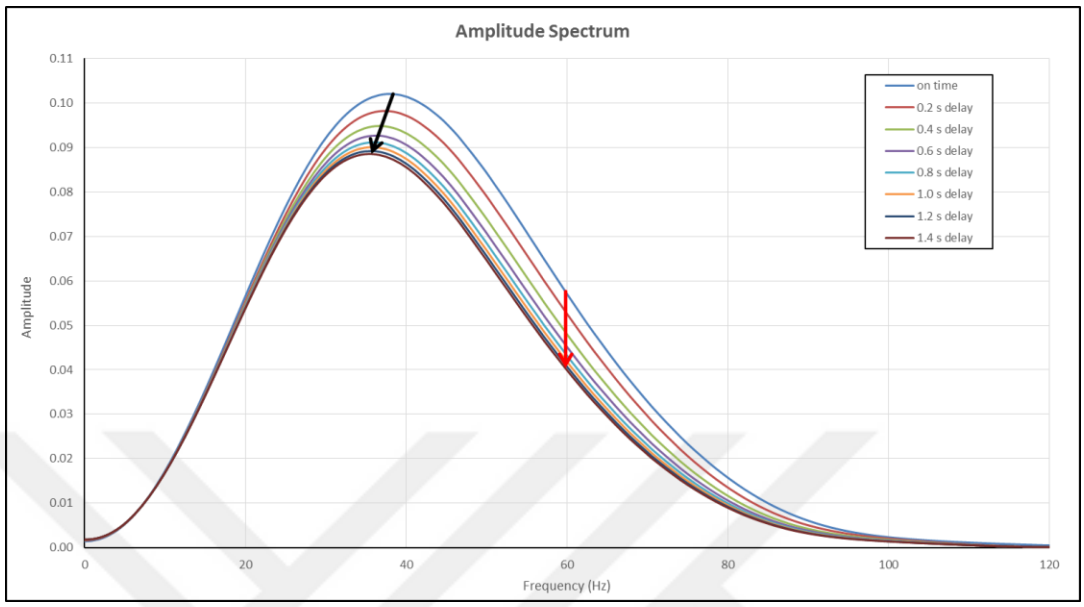

Figure 15: Amplitude spectrum result of the varying depth velocity analysis is shown in the figure. Different colors represent different time delays in the velocity analysis point. As can be seen in the figure, larger the time delay result more amplitude loss. Also, most of the lines overlap as they are at low frequencies, however, they get separated at high frequencies. Drop in the amplitude at 60 Hz is shown with the red arrow. This shows that most of the amplitude loss happens at the high frequencies. Also black arrow points out that, peak frequency shifts towards lower frequencies as the delay, thus, error, gets larger.

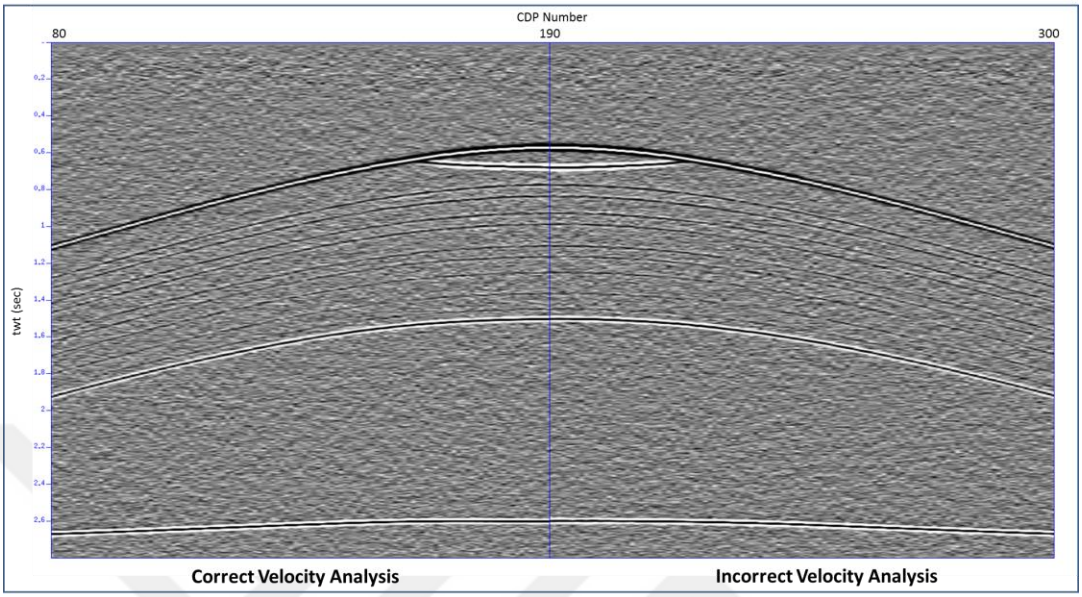

Figure 16: Resulting stacked sections of anticline model is shown in the figure. This figure consists of two different stacks of the same model. Left side is the left half of the correctly stacked section and right side is the right half of the incorrectly stacked section. Correct stacking means that a routine velocity analysis is done on the data. Incorrect stacking means that velocity profile, which comes from a velocity analysis done on a model that does not have a gas reservoir at the peak of the anticline, is used. So, on the right side, the bottom of the gas reservoir is very slightly wider than on the left side, which is caused by incorrect velocity usage for that location.

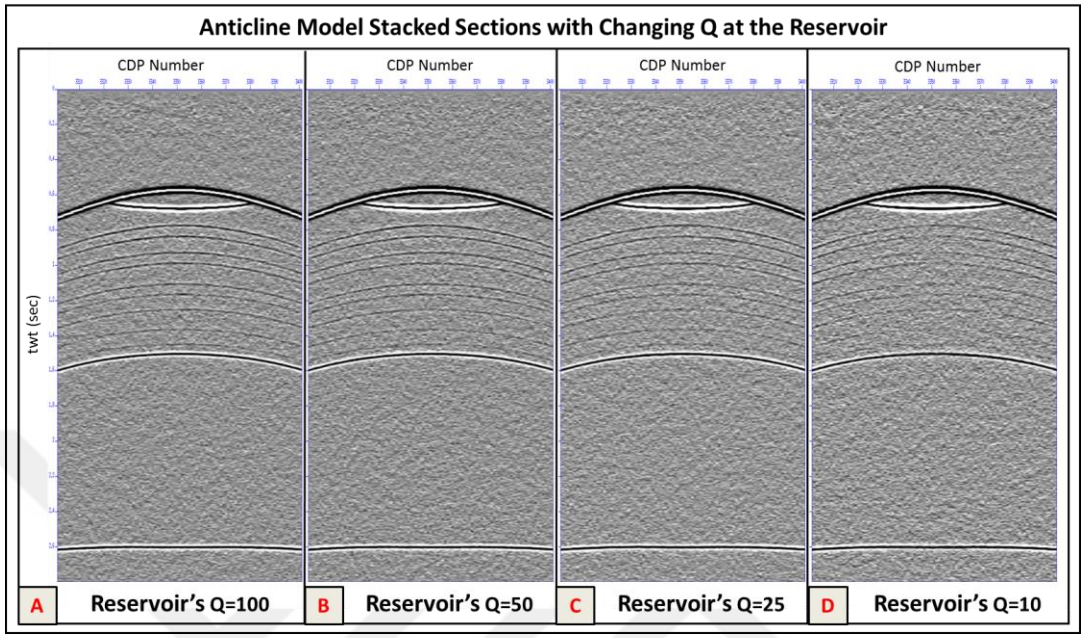

Figure 17: This figure shows the comparison of effects of different Q values on seismic data. Anticline model used for this comparison and for this image only middle portions of the stacked sections are shown. For each section reservoir area has different Q value and all other Q values are equal, and high, at all layers. (A) shows the section with reservoir Q value of 100, (B) shows the section with reservoir Q value of 50, (C) shows the section with reservoir Q value of 25 and (D) shows the section with reservoir Q value of 10. Biggest attenuation effect can be seen on the (D), since it has Q value of 10 this was expected. The important thing to notice here, once the amplitude gets attenuated, it does not recover even when the wave enters a layer with higher Q value.

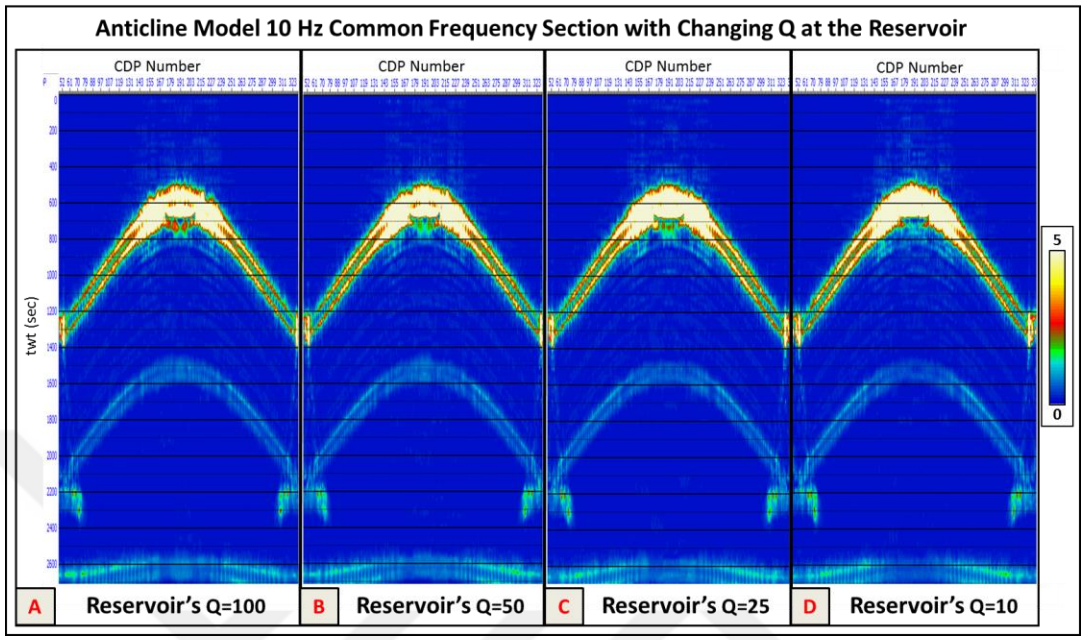

Figure 18: This image displays the anticline model's 10 Hz common frequency sections for comparison. (A) shows the model with Q value of 100 for the reservoir, (B) shows the Q=50 for reservoir and (C) is Q value of 25 for the reservoir and (D) is Q=10. Yellow and red colors are high spectral amplitude and blue is low spectral amplitude. These sections only show the spectral amplitude of a single frequency which is 10 Hz in this case. The highest attenuation occurs at the reservoir with 10 as Q value. There is still attenuation in (B) but it is not as significant as (D). Notice the low amplitude and high amplitude at the deeper reflection in (D), which is only caused by the very low Q value of the reservoir above. Thus, it shows that the amplitude does not recover even for very strong events.

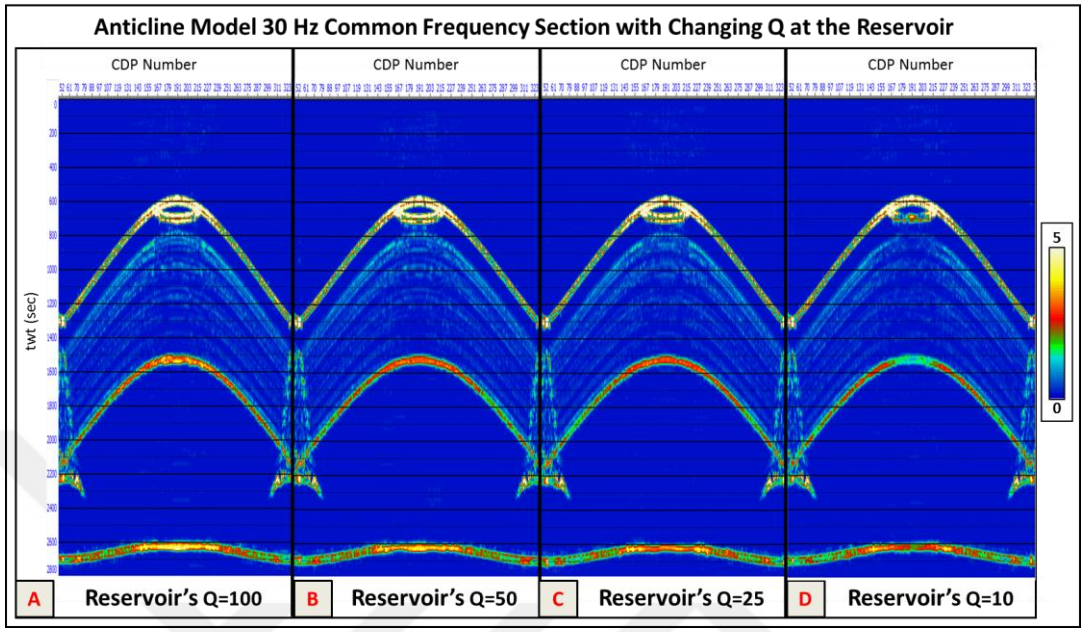

Figure 19: This image displays the anticline model's 30 Hz common frequency sections for comparison. (A) shows the model with Q value of 100 for the reservoir, (B) shows Q=50 for reservoir and (C) Q has a value of 25 for the reservoir and (D) is Q=10. Yellow and red colors are high spectral amplitude and blue is low spectral amplitude. This sections only show the spectral amplitude of a single frequency which is 30 Hz in this case. Highest attenuation occurs at the reservoir with 10 as Q value. There is still attenuation in (B) but it is not as significant as (D). Notice the low amplitude and high amplitude at the deeper reflection in (D), which is only caused by the very low Q value of the reservoir above. Attenuation is even more apparent at 30 Hz.

8. Appendices

Appendix A: Seismic Survey Parameters for Synthetic Data

Table 1: Seismic survey parameters used for the Flat Reservoir Model

Flat Reservoir Model	
Number of Receivers	60
Location of First Receiver (m)	-1475
Location of Last Receiver (m)	5425
Number of Shots	80
Location of First Shot (m)	0
Location of Last Shot (m)	3950
Sampling Interval (ms)	0.001
Number of Samples	2501
Record Length (sec)	2.5

Table 2: Seismic survey parameters used for the Varying Depth Model

Varying Depth Model	
Number of Receivers	60
Location of First Receiver (m)	-1475
Location of Last Receiver (m)	5425
Number of Shots	80
Location of First Shot (m)	0
Location of Last Shot (m)	3950
Sampling Interval (ms)	0.001
Number of Samples	3001
Record Length (sec)	3.0

Table 3: Seismic survey parameters used for the Anticline Model

Anticline	
Number of Receivers	60
Location of First Receiver (m)	-1475
Location of Last Receiver (m)	9425
Number of Shots	160
Location of First Shot (m)	0
Location of Last Shot (m)	7950
Sampling Interval (ms)	0.004
Number of Samples	701
Record Length (sec)	2.8

Appendix B: Model Parameters

Table 4: Model parameters used for the Flat Reservoir Model.

Flat Reservoir Model				
Layer #	**Name**	**Thickness (m)**	**Velocity (m/s)**	**Density (g/cm^3)**
1	*Overlaying Shale*	1000	3500	2.38
2	*Gas Sand*	200	2834	1.97
3	*Water Sand 1*	200	3165	2.17
4	*Water Sand 2*	100	3215	2.18
5	*Water Sand 3*	150	3265	2.19
6	*Water Sand 4*	100	3315	2.20
7	*Water Sand 5*	150	3365	2.21
8	*Water Sand 6*	200	3415	2.22
9	*Water Sand 7*	100	3465	2.23
10	*Water Sand 8*	150	3515	2.24
11	*Water Sand 9*	200	3565	2.25
12	*Water Sand 10*	150	3615	2.26
13	*Water Sand 11*	100	3665	2.27
14	*Underlying Shale*	1000	4000	2.47
15	*Basement*	400	6000	2.73

Table 5: Model parameters used for the Varying Depth Model.

Varying Depth Model				
Layer #	**Name**	**Thickness (m)**	**Velocity (m/s)**	**Density (g/cm^3)**
1	*Overlying Shale*	1000	3500	2.38
2	*Gas Sand*	200	2834	1.97
3	*Water Sand 1*	100	3215	2.18
4	*Water Sand 2*	1500	3265	2.19
5	*Underlying Shale*	400	3500	2.47

Table 6: Model parameters used for the Flat Reservoir Model.
Q values for Gas Sand is changed for different models.

Anticline Model					
Layer #	**Name**	**Thickness (m)**	**Velocity (m/s)**	**Density (g/cm^3)**	**Quality Factor**
1	*Overlying Shale*	1000-2200	3500	2.38	400
2	*Gas Sand*	150	2834	1.97	100 50 25 10
3	*Water Sand 1*	300	3165	2.17	400
4	*Water Sand 2*	100	3215	2.18	400
5	*Water Sand 3*	150	3265	2.19	400
6	*Water Sand 4*	100	3315	2.20	400
7	*Water Sand 5*	200	3365	2.21	400
8	*Water Sand 6*	100	3415	2.22	400
9	*Water Sand 7*	150	3465	2.23	400
10	*Water Sand 8*	200	3515	2.24	400
11	*Water Sand 9*	150	3565	2.25	400
12	*Water Sand 10*	100	3615	2.26	400
13	*Underlying Shale*	1000-2200	4000	2.47	400
14	*Basement*	400	6000	2.73	400